Rev. Adv. Mater. Sci. 52 (2017) 113-120

COLLECTIVE MIGRATION OF LOW-ANGLE TILT BOUNDARIES IN NANOCRYSTALLINE METALS UNDER FATIGUE LOADING

Ya.V. Konakov[1,2], I.A. Ovid'ko[1,2,3], A.G. Sheinerman[1,2,3] and N.V. Skiba[1,2,3]

[1]Peter the Great St. Petersburg Polytechnic University, Polytechnicheskya 29, St. Petersburg 195251, Russia
[2]Institute of Problems of Mechanical Engineering, Russian Academy of Sciences, Bolshoj 61, Vasil. Ostrov, St. Petersburg 199178, Russia
[3]Saint Petersburg State University, 7/9 Universitetskaya nab., St. Petersburg, 199034 Russia

Received: July 12, 2017

Abstract. A model is suggested that describes collective migration of two neighboring low-angle tilt boundaries in nanocrystalline metals under fatigue loading. Within the model, low-angle tilt boundaries are considered as the walls of edge lattice dislocations, while the triple junctions that terminate these boundaries contain wedge disclinations that accommodate the stress fields created by the dislocation walls. The simulation using the method of two-dimensional dislocation dynamics for the case of nanocrystalline Fe, revealed various migration modes of tilt boundaries under fatigue loading. These include the reversible migration of tilt boundaries, their split as well as their motion to adjacent high-angle grain boundaries and subsequent coalescence with these boundaries. The simulations demonstrate that the mode of boundary migration is determined by the level of the applied load and explain the recent observations of the reversible grain lattice reorientation near a crack tip in a nanocrystalline Ni-Fe alloy under fatigue loading.

1. INTRODUCTION

It is known that the unique mechanical properties of nanocrystalline (NC) metals and alloys are influenced by the plastic deformation mechanisms operating in these advanced materials [1-10]. In particular, in parallel with conventional lattice dislocation slip and deformation twinning, grain boundary (GB) deformation modes significantly contribute to plastic deformation of NC metals; see, e.g., [1-10]. At the same time, as in the case of thermally activated GB migration, their stress-driven athermal migration can lead to grain growth and, as a consequence to the degradation of mechanical or functional properties of the material [11-34].

Recently, a number of papers have been devoted to the study of GB migration and grain growth in NC metallic materials [11-20, 24-26, 28, 31-47]. In particular, Cheng et al. [33] observed reversible plastic deformation associated with reversible grain lattice reorientation near a crack tip in an NC Ni-Fe alloy under fatigue loading. They also observed the multiple transformations of high-angle GBs into low-angle ones or their complete annihilation resulting in grain growth. It is natural to assume that both these processes are associated with the collective migration and interactions of GBs. Also, the study [34] theoretically described the process of collective GB migration during plastic deformation of NC materials under a constant load. The authors of ref. [34] demonstrated, in particular, that at high enough values of the applied load collective GB migration can result in grain growth or nucleation of new nanograins. However, the theoretical model [34] does not describe the process of reversible grain lattice reorientation in NC solids under fatigue load-

Corresponding author: Ya.V. Konakov, e-mail: for-rams@yandex.ru

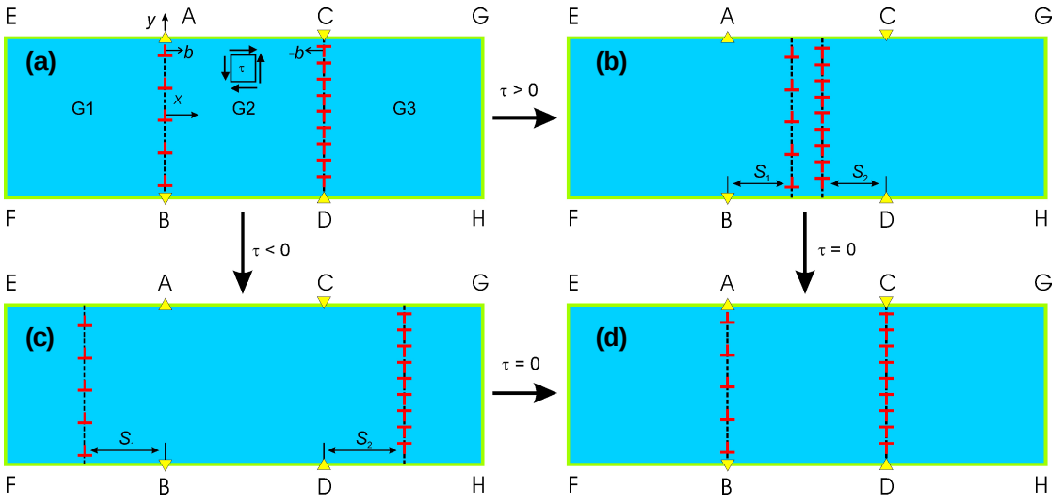

Fig. 1. Collective migration of low-angle GBs in a nanocrystalline metal under fatigue loading. (a) A two-dimensional model fragment of a nanocrystalline metal specimen consisting of a group of three square grains G1, G2 and G3 surrounded by high-angle GBs EG, GH, HF and FE and separated by low-angle GBs AB and CD. (b) and (c) Low-angle tilt boundaries AB and CD migrate under the action of a positive (b) or negative (c) resolved shear stress τ. (d) After unloading, low-angle tilt boundaries return to their initial positions.

ing. The aim of the present paper is to construct a model of athermal collective migration of two parallel low-angle GBs in NC metals under fatigue loading, to reveal various migration modes of these GBs (resulting, in particular, in reversible grain lattice reorientation or grain growth) and to approximately compute the critical parameters of the operation of a particular GB migration mode.

2. MODEL

Let us consider a model fragment of a nanocrystalline metal specimen consisting of three square grains G1, G2 and G3 separated by two low-angle tilt boundaries AB and CD (Fig. 1). The grains G1 and G3 are bounded from the left and right, respectively, by the high-angle GBs EF and GH (Fig. 1). In the initial state, the length of the GBs AB, CD, EF, GH and the distances EA, AC, CG, FB, BD and DH are equal and denoted by L. Within our model we consider tilt boundaries AB and CD as regular walls of edge perfect dislocations with opposite-sign Burgers vectors **b** and -**b** (see Fig. 1). The low-angle GBs AB and CD are characterized by tilt misorientations θ_1 and θ_2, respectively, which are related to the periods h_1 and h_2 of the dislocation walls AB and CD, respectively, by the relation: $\tan(\theta_k/2) = b/(2h_k)$, where k = 1,2. We assume that the triple junctions A, B, C and D of the GBs are balanced and contain wedge disclinations of strengths $-\omega_1$, ω_1, ω_2 and $-\omega_2$, respectively (Fig. 2), which are related to misorientation angles θ_1 and θ_2

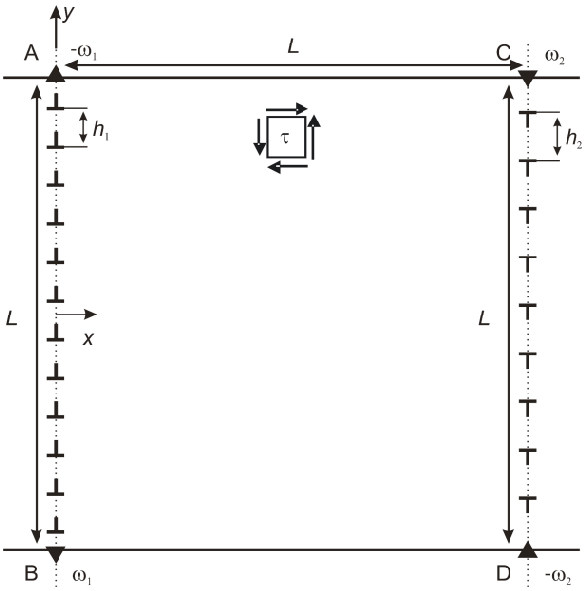

Fig. 2. Geometry of low-angle tilt boundaries AB and CD.

of the GBs AB and CD by the relation $\omega_k = \theta_k$ (k = 1,2).

Next, we consider the situation where the nanocrystalline solid is under the action of a uniaxial fatigue load, which creates an alternating resolved shear stress τ in the (x, y) plane, as shown in Fig. 1. We also focus on the case where each loading cycle involves a period of constant uniaxial loading and a period of unloading, when loading is absent. As a result, the resolved shear stress τ acts in the (x, y) plane with a constant duration at regular intervals. Then, if the resolved shear stress τ is high enough, the dislocations composing the low-angle

tilt boundaries AB and CD can both migrate under the action of the applied shear stress τ during the periods of loading and in some cases move backwards during the periods of unloading.

To describe the migration of GBs AB and CD under the action of the applied shear stress τ, we will use the method of two-dimensional dislocation dynamics in solids [48-51]. For simplicity, we assume that the process under consideration occurs at low homological temperatures and that the effects associated with thermally activated GB migration are absent. In the framework of the approach used, we will assume that each of the dislocations that compose the migrating GBs can move only along one slip plane (along the *x*-axis in Fig. 1). (In this case, if the dislocations of the boundaries AB and CD are on the same slip plane, their annihilation is possible if during the migration they approach each other.) Such one-dimensional dislocation motion can be expressed by the dependences $x_i(t)$, where x_i is the coordinate of the *i*-th dislocation ($i = 1,...,N$), N is the total number of the dislocations in the walls AB and CD, and t is time. Also, we denote the number of the dislocations in the dislocations walls AB and CD as N_1 and N_2, respectively, so that for the dislocations of the GB AB, $i = 1,\ldots,N_1$, while for the dislocations of the GB CD, $i = N_1+1,\ldots,N_1+N_2$ ($N_1 + N_2 = N$). Finally, we assume that the dislocations of the migrating boundaries AB and CD, reaching high-angle boundaries, are absorbed by them, and can no longer move.

To simulate this one-dimensional dislocation motion, we have to calculate the projection F_i on the *x*-axis of the resultant force exerted on the *i*-th dislocation by the shear stress τ, the disclinations in the triple junctions of the GBs, and the other dislocations. In the periods when there is no external stress, the motion of dislocations occurs solely as a result of their interaction with other defects of the system under consideration. Thus, in the approximation of an elastically isotropic solid with the shear modulus G and Poisson's ratio ν, the projection of total force F_i acting on the *i*-th dislocation can be expressed as follows: $F_i = b_i\tau + F_0$ during loading and $F_i = F_0$ during unloading, where $b_i = b$ for $i = 1,\ldots,N_1$, $b_i = -b$ for $i = N_1+1,\ldots, N$,

$$F_i = b_i\tau + D\sum_{\substack{k=1\\k\neq i}}^{N} b_i b_k \frac{(x_i - x_k)[(x_i - x_k)^2 - (y_i - y_k)^2]}{[(x_i - x_k)^2 + (y_i - y_k)^2]^2} - -Db_i\omega_1\left(\frac{x_i(y_i + L/2)}{x_i^2 + (y_i + L/2)^2} - \right.$$

$$\left.\frac{x_i(y_i - L/2)}{x_i^2 + (y_i - L/2)^2}\right) + Db_i\omega_2\left(\frac{(x_i - L)(y_i + L/2)}{(x_i - L)^2 + (y_i + L/2)^2} - \frac{(x_i - L)(y_i - L/2)}{(x_i - L)^2 + (y_i - L/2)^2}\right), \quad (1)$$

$D = G/(2\pi(1-\nu))$, and (x_i,y_i) are the coordinates of the *i*-th dislocation. In this case, $y_i = h_1(i-1/2)-L/2$ for $i = 1,\ldots,N_1$, and $y_i = h_2(i-1/2)-L/2$ for $i = N_1+1,\ldots, N$. The first term in Eq. (1) characterizes the total force exerted on the *i*-th dislocation by the other dislocations of the migrating GBs AB and CD. The second and third terms represent the total force of the interaction of the *i*-th dislocation with the disclinations in the triple junctions A, B, C and D.

The equations of dislocation motion have the following form [48]:

$$m\frac{d^2x_i}{dt^2} + \beta\frac{dx_i}{dt} = F_i, \quad i = 1,...,N, \quad (2)$$

where β denotes the viscosity coefficient, m is the dislocation mass defined [48] as $m = \rho b^2/2$, and ρ is the density of the material.

3. RESULTS AND DISCUSSION

Using Eqs. (1) and (2), we simulated the collective migration of two low-angle tilt boundaries under fatigue loading in nanocrystalline Fe. The following material parameters characteristic of Fe were used for the calculations: $G = 84$ GPa, $\nu = 0.29$, $b = 0.287$ nm, $\rho = 7850$ kg·m^{-3}. We also put $\omega_1 = 5°$, $\omega_1 = 4.15°$, $L = 98.7$ nm and $\beta = 5\cdot10^{-5}$ Pa·s [51]. The simulations incorporated a sequence of loading and unloading periods. During the simulation, in each loading or unloading period, dislocation motion stops when all the dislocations have reached either high-angle GBs or their equilibrium positions and then resumes when loading is replaced by unloading or visa verse.

Using the above simulation procedure, we calculated the profiles of low-angle GBs during the migration process at different values of the periodically acting shear stress τ. In the case $\tau > 0$, where the GBs AB and

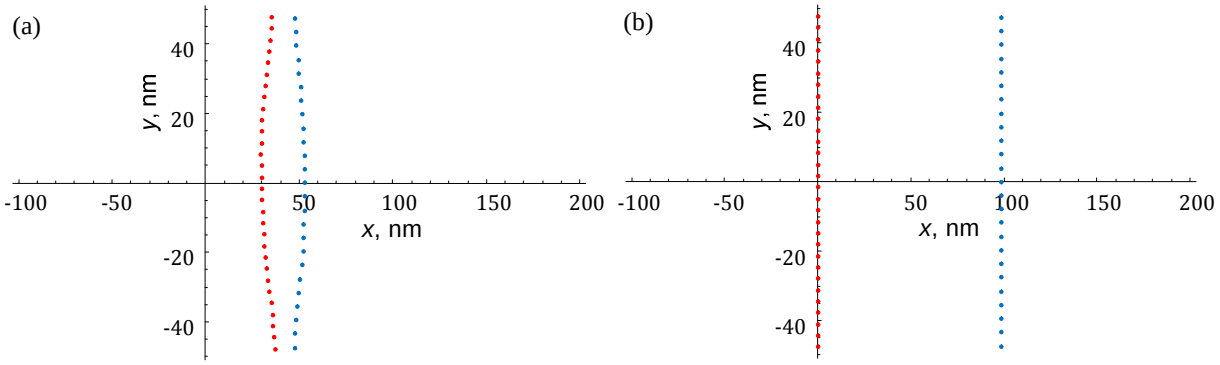

Fig. 3. The profiles of the migrating low-angle GBs in the first migration mode, for $\tau = 1.2$ GPa. (a) During loading, the migrating GBs reach their equilibrium positions. (b) Upon unloading, the GBs return to their initial equilibrium positions. Here and in the following figures the red dots specify the dislocations with the Burgers vector **b** (that initially compose the GB AB) while the blue dots depict the dislocations with the Burgers vector -**b** (that initially compose the GB CD).

CD migrate towards each other during loading, we revealed four characteristic migration modes. In the first mode (Fig. 3a), the two low-angle GBs during the stress driven migration move towards each other during loading but do not reach each other. In this mode, all the dislocations composing the migrating GBs move to their equilibrium positions (Fig. 3a). This mode is realized at relatively low values of τ. When the applied stress disappears, both low-angle GBs return to their initial positions (Fig. 3b).

Let us denote the average distances traversed by the dislocations of the GB AB and CD during loading as S_1 and S_2, respectively. The dependences of S_1 and S_2 on the resolved shear stress τ are presented in Fig. 4. This figure demonstrates that S_1 and S_2 increase with τ. As a result, at high enough values of τ, the sum average migration distance S_1+S_2 becomes close to the initial spacing L between the low-angle GBs. In this case, if all or some dislocations of the GBs AB and CD are on the same slip planes, the dislocations located on the same slip planes can annihilate. (This case is trivial and we will not consider it in the following.) In contrast, if all the dislocations of the GBs AB and CD lie at different slip planes, some of the moving dislocations pass through the walls of opposite-sign dislocations and move to high-angle GBs (Fig. 5a).

Thus, with an increase of the shear stress, a transition from the first to the second migration mode takes place (Fig. 5a). The second migration mode is characterized by the passage of a part of moving dislocations to the right and left high-angle GBs. In this mode, the remaining moving dislocations reach equilibrium positions (Fig. 5a). After unloading, the latter tend to return to their initial positions (Fig. 5b). In some cases, in subsequent loading periods, new dislocations can move to high-angle GBs (Fig.

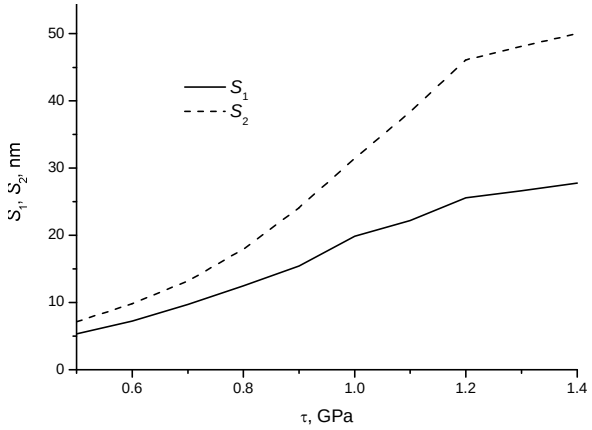

Fig. 4. The dependences of the average dislocation migration distances S_1 and S_2 on the shear stress τ.

5c). However, after several cycles of loading, new dislocations do not reach high-angle GBs any more and move back and forth during the loading and unloading periods.

The average migration distances S_1 and S_2 (defined as the average distances between the positions of dislocations after the loading period of the p-th loading cycle and their initial positions before the first loading cycle) passed by the dislocations of the GB AB and CD, respectively, as functions of the number p of the loading cycles are plotted in Fig. 6. Figure 6 demonstrates that S_1 and S_2 first increase with p and then, after several loading cycles, approach constant levels.

With a further increase of the shear stress, the third migration mode is realized (Fig. 7). In this mode, during the migration, low-angle GBs penetrate each other. After that the fragmentation of the GB with the lower misorientation occurs. As a result, this GB is divided into three segments. The central segment, attracted by the GB with the greater

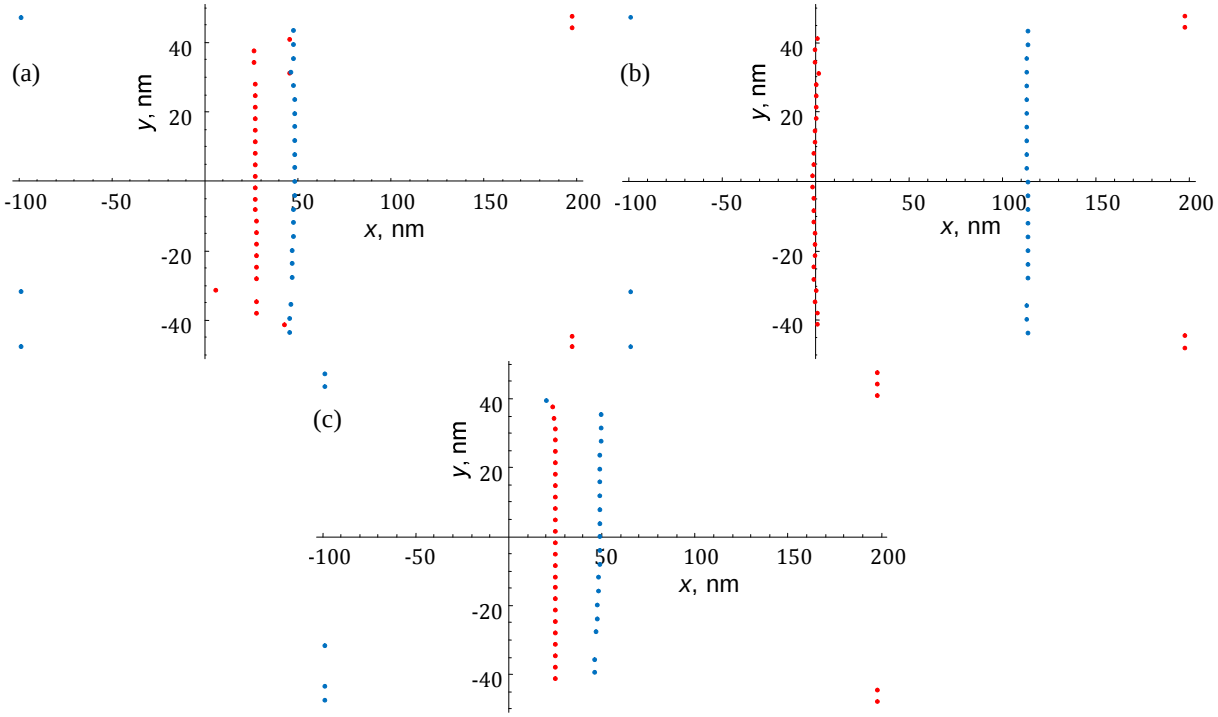

Fig. 5. The profiles of the migrating low-angle GBs in the second migration mode, for $\tau = 1.7$ GPa. (a) Upon loading in the first loading cycle, all the dislocations reach their equilibrium positions or high-angle GBs. (b) Upon unloading in the first loading cycle, all the dislocations not absorbed by high-angle GBs return to their initial positions. (c) Upon loading in the fourth loading cycle, the profiles are nearly the same as after loading in the first loading cycle.

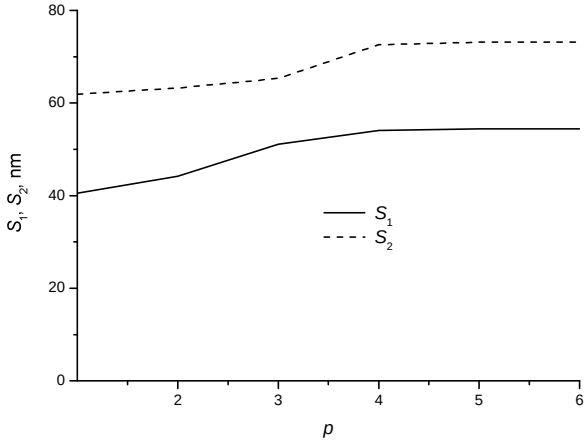

Fig. 6. Average dislocation migration distances S_1 and S_2 in the second migration mode as functions of the number p of loading cycles, for $\tau = 1.7$ GPa.

misorientation, begins to move in the opposite direction (to the right) until its dislocations reach their equilibrium positions. The remaining dislocations of the migrating GBs under consideration reach high-angle GBs (Fig. 7a). After unloading, the central segment of the split GB migrates to the right high-angle GB (Fig. 7b). As a result, all the dislocations of the migrating GBs are captured by the high-angle GBs, and the grains G1, G2 and G3 are united into one.

With a further increase of the resolved shear stress t, the transition occurs from the third to the fourth migration mode. In the fourth migration mode, both low-angle GBs pass through each other and reach high-angle GBs (Fig. 8). Like the third migration mode, in this situation, the three grains under consideration (G1, G2 and G3) unite into one.

Now consider the case $\tau < 0$, when the low-angle GBs AB and CD migrate away from each other during loading. As in the case $\tau > 0$ examined above, for not too high absolute values of τ, both GBs migrate there and back during loading and unloading, respectively (Fig. 9). (We denote such reversible GB motion as the fifth migration mode.) With an increase of the absolute value of the shear stress τ, the transition to the sixth migration mode occurs, which is characterized by migration of the low-angle GB with the lower misorientation to the nearest high-angle GB. In this mode, the dislocations of the second low-angle GB reach their equilibrium positions (Fig. 10a). After unloading, this GB tends to return to its initial position (Fig. 10b), and its dislocations reach new equilibrium positions near the initial positions before the migration. Thus, with the successive emergence and disappearance of the applied load, this mode is characterized by the coa-

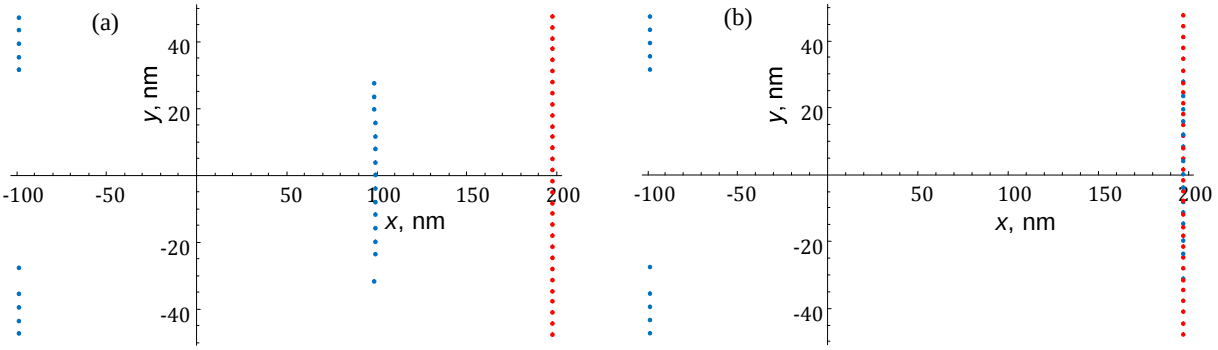

Fig. 7. The profiles of the migrating low-angle GBs in the third migration mode, for $\tau = 2.7$ GPa. (a) Upon loading, the low-angle GBs pass through each other. Then the GB with the higher misorientation approaches a high-angle GB and merges with it. The GB with the lower misorientation splits, and its upper and lower parts approach a high-angle GB and merge with it, while its central fragment reaches its equilibrium position. (b) Upon unloading, the central fragment of the split GB with the lower misorientation approaches the nearest high-angle GB and merges with it.

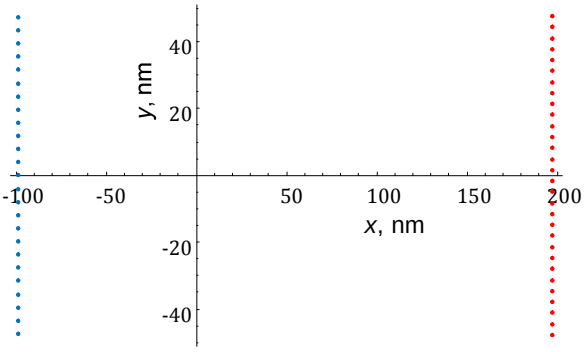

Fig. 8. The profiles of the migrating low-angle GBs in the fourth migration mode, for $\tau = 2.8$ GPa. Upon loading, the GBs pass through each other and then move to the nearest high-angle GBs and merge with them.

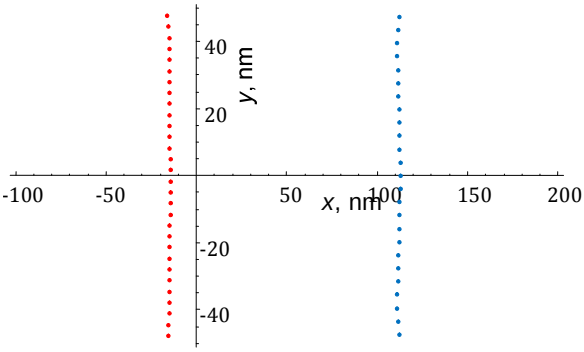

Fig. 9. Typical profiles of the migrating low-angle GBs in the fifth migration mode, for $\tau = -0.5$ GPa. During loading, the migrating GBs reach their equilibrium positions.

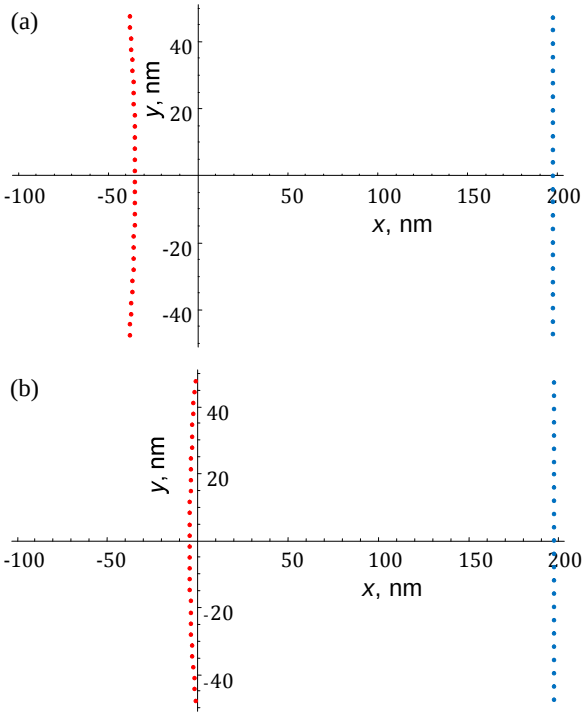

Fig. 10. The profiles of the migrating low-angle GBs in the sixth migration mode, for $\tau = -1$ GPa. (a) Upon loading, the GB with the lower misorientation moves to the nearest high-angle GB and merges with it, while the GB with the higher misorientation migrates to its equilibrium position. (b) Upon unloading, the GB with the higher misorientation returns to its initial position.

lescence of the GB with the lower misorientation with the nearest high-angle GB and the reversible migration of the GB with the higher misorientation.

At $\tau < 0$ and the highest absolute values of τ, the seventh migration mode is realized. In this mode, both low-angle GBs reach the nearest high-angle GBs (Fig. 11). This migration mode is analogous to the fourth migration mode. The sixth and seventh regimes are realized at significantly lower absolute values of the shear stress τ than the fourth migration mode. This is related to the weaker attraction of the dislocations of different migrating low-angle

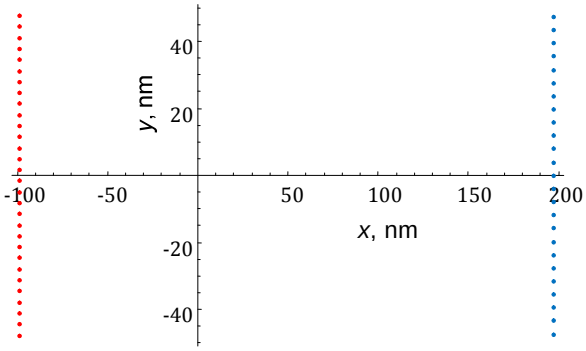

Fig. 11. The profiles of the migrating low-angle GBs in the seventh migration mode, for τ = -1.2 GPa. Upon loading, the GBs move to the nearest high-angle GBs and merge with them.

GBs in the case $\tau < 0$ (where the low-angle GBs move away from each other) than in the case $\tau > 0$ (where the low-angle GBs initially move towards each other).

4. CONCLUSIONS

In this paper we have used the method of two-dimensional dislocation dynamics to simulate the collective migration of two small-angle GBs in NC metals under fatigue loading. As a result, a number of migration modes was revealed. Depending on the sign and level of the shear stress, the considered GBs can reversibly migrate (Figs. 3 and 9), move to the high-angle GBs (Figs. 8 and 11) or and split (Fig. 7) and in some cases pass through each other (Figs. 7 and 8). At small or moderate absolute values of the resolved shear stress τ, the low-angle GBs reversibly migrate, and their characteristic migration lengths increase with the absolute value of τ (Fig. 4). Such reversible migration of adjacent GBs during fatigue loading has recently been documented [33] near a crack tip in a nanocrystalline NiFe alloy. At a higher absolute values of τ, one or both low-angle GBs move to, and merge with the neighboring high-angle GBs, thereby leading to local grain growth. Also, when the resolved shear stress τ drives the low-angle GBs to migrate towards each other, the latter can (at sufficiently high values of τ) pass through each other, resulting in the disappearance of the initial grain and nucleation of a new one. Alternatively, in the special where the examined GBs have the same misorientations, the dislocations composing the neighboring low-angle GBs can lie in the same slip plane. In this special case, the low-angle GBs can completely annihilate when they meet, thus leading to local grain growth.

ACKNOWLEDGEMENTS

N.V.S. acknowledges the support of the Russian Ministry of Education and Science (grant MD-9152.2016.1) and the Russian Fund of Basic Research (grant 16-32-60110). Ya.V.K. and A.G.S. acknowledge the support of the Russian Ministry of Education and Science (task 16.3483.2017/PCh).

REFERENCES

[1] A.K. Mukherjee // *Mater. Sci. Eng. A* **322** (2002) 1.
[2] I.A. Ovid'ko // *Int. Mater. Rev.* **50** (2005) 65.
[3] M. Kawasaki and T.G. Langdon // *J. Mater. Sci.* **42** (2007) 1782.
[4] M. Dao, L. Lu, R.J. Asaro, J.T.M. De Hosson and E. Ma. // *Acta Mater.* **55** (2007) 4041.
[5] C.S. Pande and K.P. Cooper // *Progr. Mater. Sci.* **54** (2009) 689.
[6] J. Monk and D. Farkas // *Phys. Rev. B* **75** (2007) 045414.
[7] I.A. Ovid'ko and T.G. Langdon // *Rev. Adv. Mater. Sci.* **30** (2012) 103.
[8] R.Z. Valiev, I. Sabirov, A.P. Zhilyaev and T.G. Langdon // *JOM* **64** (2012) 641134.
[9] Y.T. Zhu, X.Z. Liao and X.-L. Wu // *Progr. Mater. Sci.* **57** (2012) 1.
[10] Y. Estrin and A. Vinogradov. Acta Mater // **61** (2013) 782.
[11] M. Jin, A.M. Minor, E.A. Stach and J.W. Morris Jr // *Acta Mater.* **52** (2004) 5381.
[12] W.A. Soer, J.T.M. De Hosson, A.M. Minor, J.W. Morris Jr and E.A. Stach // *Acta Mater.* **52** (2004) 5783.
[13] M.Y. Gutkin and I.A. Ovid'ko // *Appl. Phys. Lett.* **87** (2005) 251916.
[14] F. Sansoz and V. Dupont // *Appl. Phys. Lett.* **89** (2006) 111901.
[15] D. Pan, T.G. Nieh and M.W. Chen // *Appl. Phys. Lett.* **88** (2006) 161922.
[16] P.L. Gai, K. Zhang and J. Weertman // *Scripta Mater.* **56** (2007) 25.
[17] V. Dupont and F. Sansoz // *Acta Mater.* **56** (2008) 6013.
[18] I.A. Ovid'ko, A.G. Sheinerman and E.C. Aifantis // *Acta Mater.* **56** (2008) 2718.
[19] T.J. Rupert, D.S. Gianola, Y. Gan and K.J. Hemker // *Science* **326** (2009) 1686.
[20] S. Cheng, Y. Zhao, Y. Wang, Y. Li, X.-L. Wang, P.K. Liaw and E.J. Lavernia // *Phys. Rev. Lett.* **104** (2010) 255501.
[21] S.V. Bobylev, N.F. Morozov and I.A. Ovid'ko // *Phys. Rev. Lett.* **105** (2010) 055504.

[22] S.V. Bobylev, N.F. Morozov and I.A. Ovid'ko // *Phys. Rev. B* **84** (2011) 094103.
[23] I.A. Ovid'ko, A.G. Sheinerman and E.C. Aifantis // *Acta Mater.* **59** (2011) 5023.
[24] S.V. Bobylev and I.A. Ovid'ko // *Acta Mater.* **88** (2015) 260.
[25] Y. Lin, H., Wen, Y. Li, B. Wen and E.J. Lavernia // *Metall. Mater. Trans. B* **45** (2014) 795.
[26] Y. Lin, B. Xu, Y. Feng nd E.J. Lavernia // *J. Alloys Compd.* **596** (2014) 79.
[27] K. Dám and P. Lejček // *Mater. Charact.* **76** (2013) 69.
[28] Y. Lin, H. Wen, Y. Li, B. Wen, L. Wei and E.J. Lavernia // *Acta Mater.* **82** (2015) 304.
[29] T. Zálezák and A. Dlouhý // *Acta Phys. Pol. A* **122** (2012) 450.
[30] I.A. Ovid'ko and A.G. Sheinerman // *Rev. Adv. Mater. Sci.* **39** (2014) 99.
[31] I.A. Ovid'ko and A.G. Sheinerman // *J. Mater. Sci.* **50** (2015) 4430.
[32] Ya.V. Konakov, I.A. Ovid'ko and A.G. Sheinerman // *Mater. Phys. Mech.* **24** (2015) 97.
[33] S. Cheng, S.Y. Lee, L. Li, C. Lei, J. Almer, X.-L. Wang, T. Ungar, Y. Wang and P.K. Liaw // *Phys. Rev. Lett.* **110** (2013) 135501.
[34] M.Yu. Gutkin, K.N. Mikaelyan and I.A. Ovid'ko // *Phys. Solid State* **50** (2008) 1266.
[35] K. Zhang, J.R. Weertman and J.A. Eastman // *Appl. Phys. Lett.* **85** (2004) 5197.
[36] K. Zhang, J.R. Weertman and J.A. Eastman // *Appl. Phys. Lett.* **87** (2005) 061921.
[37] D. Farkas, A. Froseth, H. Van Swygenhoven // *Scr. Mater*. **55** (2006) 695.
[38] J.T.M. De Hosson, W.A. Soer, A.M. Minor, Z.W. Shan, E.A. Stach, S.A.S. Asif and O.L. Warren // *J. Mater. Sci.* **41** (2006) 7704.
[39] D.S. Gianola, S. Van Petegem, M. Legros, S. Brandstetter, H. Van Swygenhoven and K.J. Hemker // *Acta Mater.* **54** (2006) 2253.
[40] D.S. Gianola, D.H. Warner, J.F. Molinari and K.J. Hemker // *Scr. Mater.* **55** (2006) 649.
[41] X.Z. Liao, A.R. Kilmametov, R.Z. Valiev, H.S. Gao, X.D. Li, A.K. Mukherjee, J.F. Bingert and Y.T. Zhu // *Appl. Phys. Lett.* **88** (2006) 021909.
[42] G.J. Fan, Y.D. Wang, L.F. Fu, H. Choo, P.K. Liaw, Y. Ren and N.D. Browning // *Appl. Phys. Lett.* **88** (2006) 171914.
[43] D. Pan, S. Kuwano, T. Fujita and M.W. Chen // *Nano Lett.* **7** (2007) 2108.
[44] J.A. Sharon, P.-C. Su, F.B. Prinz and K.J. Hemker // *Scr. Mater.* **64** (2011) 25.
[45] D.S. Gianola, D. Farkas, M. Gamarra and M.R. He // *J. Appl. Phys.* **112** (2012) 124313.
[46] M. Aramfard and C. Deng // *Model. Simul. Mater. Sci. Eng.* **22** (2014) 055012.
[47] L. Wang, T. Xin, D. Kong, X. Shu, Y. Chen, H. Zhou H, J. Teng, Z. Zhang, J. Zou and X. Han // *Scr. Mater.* **134** (2017) 95.
[48] S.V. Bobylev, M.Yu. Gutkin, I.A. Ovid'ko // *J. Phys. D* **37** (2004) 269.
[49] S.V. Bobylev, M.Yu. Gutkin, I.A. Ovid'ko // *Acta Mater.* **52** (2004) 3793.
[50] E.A. Rzhavtsev, M.Yu. Gutkin // *Scripta Mater.* **100** (2015) 102.
[51] U.F. Kocks, A.S. Argon, M.F. Ashby // *Progr. Mater. Sci.* **19** (1975) 1.